

Erdheim-Chester Disease: MR Imaging, Anatomic, and Histopathologic Correlation of Orbital Involvement

Marcelo R. de Abreu, Christine B. Chung, Sandip Biswal, Parvis Haghighi, John Hesselink, and Donald Resnick

Summary: Erdheim-Chester disease (ECD) is a rare form of histiocytosis of unknown origin characterized by tissue infiltration by lipid-laden histiocytes. Typically, the diaphyseal and metaphyseal portions of the tubular bones are affected, leading to a characteristic radiographic pattern of bone sclerosis. Orbital involvement is not infrequent and is manifested by exophthalmos and periorbital xanthomatous lesions, with associated visual problems. This case report documents imaging and pathologic findings in a patient with ECD with extensive orbital involvement.

Erdheim-Chester disease (ECD) is a rare disease of unknown etiology characterized by multisystem involvement of infiltration of tissues by lipid-laden histiocytes (1). Patients usually present with bone pain in the 4th to 5th decades of life. This disease is characterized by typical radiologic findings of bilateral and symmetric sclerosis of the diaphysis and metaphysis of the tubular bones with sparing of the axial skeleton (2). The radiologic findings usually allow differentiation of ECD and Langerhan cells histiocytosis, although these entities share similar histologic findings.

The most frequent central nervous system manifestations of the ECD disease are diabetes insipidus, cerebellar syndromes, orbital lesions, and extra-axial dural masses (3). Infiltration of retro-orbital tissues may lead to exophthalmos, double vision, and ocular motility problems.

Case Report

ECD was diagnosed in a 52-year-old man the age of 48 years. Clinical manifestations included exophthalmos, periorbital lipid deposition (xanthomata), and chronic and progressive bone pain. The onset of the disease was characterized by periorbital xanthomas. Over a period of 2 years, his vision deteriorated and his eyes protruded to the point that he could not close his eyelids. The patient subsequently lost almost all

vision in his right eye, and vision in the left eye became progressively worse. Treatment consisted of corticosteroid injection directly into the retro-orbital region of both eyes, which led to intermittent improvement of vision.

During the course of the disease, the patient underwent several MR imaging examinations of the orbits that documented retro-orbital intraconal and extraconal deposition of abnormal tissue. This abnormal tissue revealed low signal intensity on T1-weighted spin-echo (SE) images and low signal intensity on T2-weighted fast SE images (Fig 1). The maxilla and the mandible were enlarged with replacement of the marrow by abnormal tissue.

Radiographic examination showed the typical bone alterations of the disease, with bilateral and symmetric sclerotic lesions along the diaphysis and metaphysis of tubular bones such as the femur, tibia, fibula, humerus, radius, and ulna. MR imaging examinations of the appendicular skeleton showed replacement of the normal marrow by an infiltrative process involving the diaphyses, metaphyses, and portions of epiphysis in the femur, tibia, humerus, radius, and ulna (Fig 2). An abdominal MR examination demonstrated retroperitoneal masses with decreased signal intensity in all MR imaging sequences.

Renal failure due to retroperitoneal fibrosis and ureteral obstruction caused by ECD led to the patient's death at 52 years of age. The family donated his body for radiology research.

Postmortem MR Imaging and Pathologic Findings

High-resolution MR images of the orbits were acquired with a 1.5-T superconducting MR imager (Signa; GE Medical Systems, Milwaukee, WI) with a quadrature head coil (Flex Coil; Medical Advances, Milwaukee, WI). Imaging was performed in the coronal, transverse, and sagittal planes. The MR imaging protocol consisted of a T1-weighted SE sequence (TR/TE, 600/20). To acquire a higher resolution, a section thickness of 3 mm 1 mm skip, and a small field of view of 10 × 10 cm were used. The data acquisition matrix was 256 × 192. No T2-weighted images were acquired after death because of the expected loss of tissue water. Antemortem T1-weighted images and T2-weighted images with fat suppression were compared with the postmortem T1-weighted images.

MR imaging showed bilateral retro-orbital intraconal and extraconal abnormal tissue revealing low signal intensity in postmortem and antemortem T1-weighted images and low signal intensity in antemortem T2-weighted images. The abnormal intraconal tissue replaced the normal retro-orbital fat in the center of the intraconal space, surrounding the optic nerve. There was no involvement of the extraocular muscles. The abnormal extraconal tissue was more prominent in the superolateral aspect of the eye with infiltration of the lacrimal gland. Disease anterior to the orbital septum was also noted (Figs 1 and 3A).

After MR imaging, the cadaveric specimen was frozen at –60°C for more than 96 hours and was subsequently sectioned

Received July 2, 2003; accepted after revision July 12.

From the Department of Radiology, Hospital Mae de Deus e Mae de Deus Center, Porto Alegre, Brazil (M.R.d.A.) and the Department of Radiology, University of California, San Diego, and Veterans' Administration Health Care System, La Jolla, CA (C.B.C., S.B., P.H., J.H., D.R.).

Address correspondence to Christine B. Chung, MD, Department of Radiology, University of California, San Diego, and Veterans' Administration Health Care System, 3350 La Village Dr., La Jolla, CA 92161.

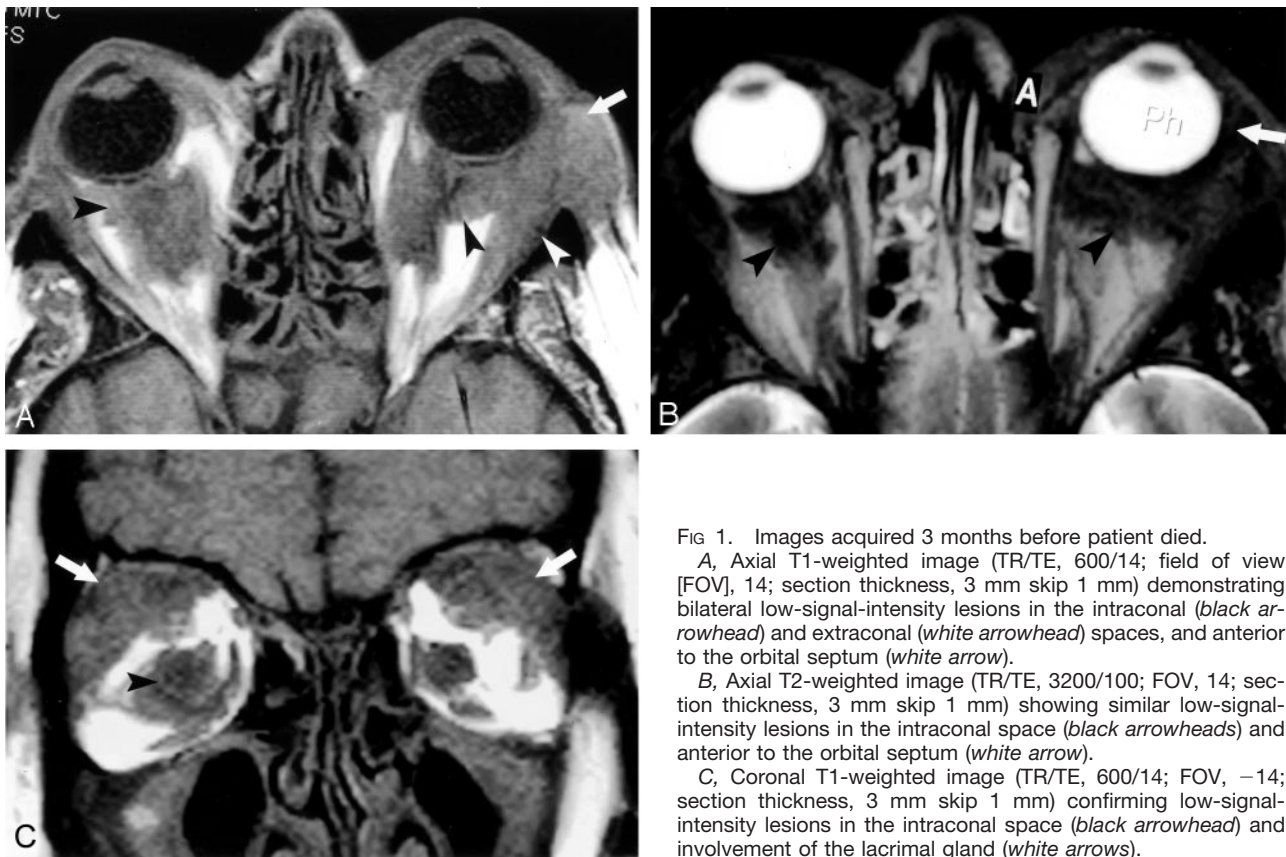


FIG 1. Images acquired 3 months before patient died.

A, Axial T1-weighted image (TR/TE, 600/14; field of view [FOV], 14; section thickness, 3 mm skip 1 mm) demonstrating bilateral low-signal-intensity lesions in the intraconal (black arrowhead) and extraconal (white arrowhead) spaces, and anterior to the orbital septum (white arrow).

B, Axial T2-weighted image (TR/TE, 3200/100; FOV, 14; section thickness, 3 mm skip 1 mm) showing similar low-signal-intensity lesions in the intraconal space (black arrowheads) and anterior to the orbital septum (white arrow).

C, Coronal T1-weighted image (TR/TE, 600/14; FOV, -14; section thickness, 3 mm skip 1 mm) confirming low-signal-intensity lesions in the intraconal space (black arrowhead) and involvement of the lacrimal gland (white arrows).

with a band saw into 3-mm-thick sections along the axial plane so that anatomic sections corresponded closely to the axial MR imaging plane. Each section was photographed and imaged with high-resolution radiography (Faxitron; Hewlett Packard, McMinnville, OR).

The anatomic sections showed infiltrative disease in the same areas as those demonstrated by MR imaging. The diseased retro-orbital intraconal and extraconal spaces revealed yellow-white discoloration with optic nerve encasement. The high-resolution radiographs of the anatomic sections showed increased radiolucent lesions that corresponded to those evident in the cadaveric tissues (Fig 3B).

Histologic analysis revealed retro-orbital tissue infiltration with very dense collagen tissue that was associated with extensive aggregates of foamy cells (macrophages). The retro-orbital fat was almost totally replaced by this infiltrative process, which extended further to involve the globe and the extraocular muscles. The pathologic tissue entrapped vessels and nerves of the retro-orbital space. The optic nerve showed abnormal foamy macrophages (Fig 3C-E).

Discussion

ECD is a rare non-Langerhan cell histiocytosis first described by Jacob Erdheim and William Chester in 1930 (4) and subsequently reported on by Jaffe in 1972 (5). The disease is characterized by tissue infiltration by lipid-laden macrophages, multinucleated giant cells, and inflammatory cells composed of lymphocytes and histiocytes, typically in the bone marrow, but also in numerous other organs (5). Until 1983, a total of 47 cases of ECD had been reported in the literature (6). Currently, about 80 cases have been

reported. Orbital involvement has been reported in only 23 of these cases (3).

For differential diagnosis and therapeutic purposes, it is important to localize the specific orbital compartment affected by the disease. MR imaging is useful for this purpose. Our study showed involvement of the anterior compartment, anterior to the orbital septum, and the posterior compartment of the orbit. In the posterior compartment, there was infiltration of the intraconal space, with replacement of the retro-orbital fat by abnormal tissue, which led to encasement of the optic nerve, and the extraconal space, with possible involvement of the lacrimal gland. It is interesting that histologic analysis showed infiltration by the disease inside structures that were interpreted as normal at MR imaging, such as the optic nerve and the extraocular muscles.

Bilateral exophthalmos, evident in this patient, is commonly encountered in Grave disease, the most common cause of bilateral proptosis. In Grave disease, however, the extraocular muscles are swollen, especially in the muscle body, a finding not evident in this case. Sarcoid and leukemia can cause bilateral exophthalmos with infiltration of multiple compartments of the eyes as seen in this case. A nonspecific inflammation of the retro-orbital tissue termed "orbital pseudotumor" shows some similarity to the imaging findings in EDC. In orbital pseudotumor, there is also infiltration of the intraconal and extraconal space, particularly of the retrobulbar fat. Orbital



FIG 2. Coronal T1-weighted image of the elbow demonstrating the replacement of normal bone marrow by low-signal-intensity, diffuse lesions (*white arrows*) in the humerus, radius, and ulna. High-signal-intensity, normal fatty marrow is spared in portions of the epiphysis of those bones (*white arrowheads*).

pseudotumor usually causes unilateral exophthalmos (7). On pathologic examination, the main differential diagnosis is Langerhan cell histiocytosis. In Langer-

han cell histiocytosis, the histiocytes are characterized by the presence of Birbeck granules on electron microscopy, and on immunohistologic examination they show a positive reaction to monoclonal antibodies OKY6 and S100 (1, 8).

Treatment of the disease includes oral steroids and, at advanced stages, chemotherapy, radiation therapy, or immunotherapy. The overall prognosis is difficult to assess, because so few cases have been reported, but the average reported survival has been 32 months after the initial diagnosis (1). The main causes of death are respiratory distress, pulmonary fibrosis, and heart failure.

The comparison of findings derived from radiography and MR imaging with those of macropathologic analysis in our patient demonstrated correspondent sites of involvement. Histologic analysis, however, revealed that the disease was much more extensive than it appeared with MR imaging and radiography.

References

1. Veysier-Belot C, Cacoub P, Caparros-Lefebvre D, et al. **Erdheim-Chester disease: clinical and radiological characteristics of 59 cases.** *Medicine (Balt)* 1996;75:157-169
2. Breuil V, Brocq O, Pellegrino C, et al. **Erdheim-Chester disease: typical bone features for a rare xanthogranulomatosis.** *Ann Rheum Dis* 2002;61:199-200
3. Wright RA, Hermmann RC, Parisi JE. **Neurological manifestations of Erdheim-Chester disease.** *J Neurol Neurosurg Psychiatry* 1999;66:72-75
4. Chester W. **Uber Lipoidgranulomatose.** *Virchows Archiv* 1930;279:561-602
5. Jaffe HL. *Metabolic, Degenerative and Inflammatory Diseases of Bones and Joints.* Munich: Urban and Schwarzenberg;1970:531-541
6. Alper MG, Zimmerman LE, Piana FG. **Orbital manifestation of Erdheim-Chester disease.** *Trans Am Ophthalmol Soc* 1983;81:64-85
7. Roden DT, Savino PJ, Zimmerman RA. **Magnetic resonance imaging in orbital diagnosis.** *Radiol Clin North Am* 1988;26:535-545
8. Soler P, Chollet S, Jacque C, et al. **Immunocytochemical characterization of pulmonary histiocytosis X cells in lung biopsies.** *Am J Pathol* 1985;118:439-451

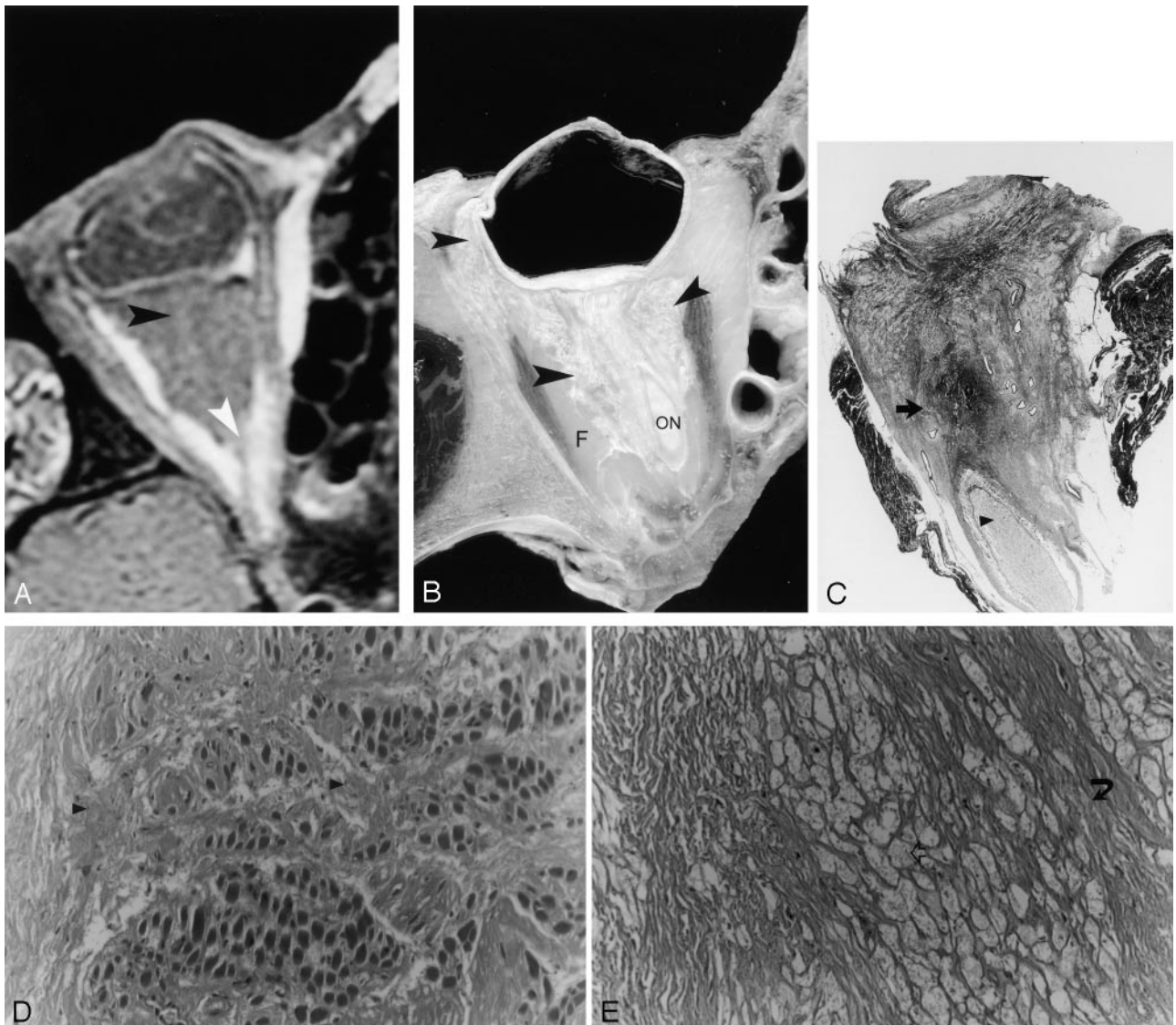


FIG 3. Postmortem correlation with MR imaging, cadaveric sections, and histology.

A, Axial T1-weighted MR imaging (TR/TE, 600/20; FOV, 10; matrix, 256×196 ; section thickness, 3 mm skip 1 mm) showing low-signal-intensity lesions of the right orbit in the intraconal space (*black arrowhead*). The normal retro-orbital fat is replaced by abnormal diseased tissue and the optic nerve is encased (*white arrowhead*). The extraocular muscles do not show any apparent alteration.

B, Cadaveric section showing the infiltrative disease (*black arrowhead*) at locations corresponding to the locations found with MR imaging. F+, retro-orbital fat; ON, optic nerve.

C, Macropathology demonstrating abnormal replacement of the retro-orbital fat by a dense fibrous material and conglomerates of lipid-laden macrophages (*black arrow*), which encase the optic nerve (*black arrowhead*). Hematoxylin and eosin preparation.

D, Histology with high magnification (magnification $\times 200$) showing involvement of the muscular interstitial space by attenuated fibrous material (*black arrowhead*).

E, Histology with high magnification (magnification $\times 100$) demonstrating the characteristic lipid-laden macrophages of ECD (*open arrow*).